PHYSICAL REVIEW A **80**, 061403(R) (2009)

Laser-induced electron diffraction in H_2 with linear and circular polarization ultrashort XUV laser pulses

Kai-Jun Yuan, HuiZhong Lu, and André D. Bandrauk*
Laboratoire de Chimie Théorique, Faculté des Sciences, Université de Sherbrooke, Sherbrooke, Québec, Canada J1K 2R1
(Received 28 September 2009; published 17 December 2009)

Numerical solution of the time-dependent Schrödinger equation for a two-dimension model of H_2 ionization by intense ultrashort (few cycles) extreme ultraviolet (XUV) laser pulses are presented to compare linear and circular polarization angular distributions for aligned molecules. Both ground ($X\ ^1\Sigma_g^+$) and excited ($A\ ^3\Sigma_u^+$) states ionization is calculated at equilibrium and for extended large internuclear distance configurations to study the effect of electron delocalization via molecular orbitals vs electron localization in Heitler-London atomic wave functions. It is found that at large distance for ionized electron wavelengths less than the internuclear distance, circular polarization ionization angular distributions exhibit signature of the entanglement of electrons by exchange, thus, allowing for a measure of exchange entanglement.

DOI: 10.1103/PhysRevA.80.061403 PACS number(s): 33.80.Eh, 42.25.Fx

Recent advances in the synthesis and characterization of ultrashort intense laser pulses [1,2] allows for investigation of laser-matter interaction into a new temporal regime leading to attosecond science [3,4], thus, bridging near femtosecond (1 fs=10^{-15} s) dynamics of proton motion to attosecond (1 as=10^{-18} s) dynamics of electrons. Imaging quantum dynamics is as a result a frontier of science which is being developed and advanced through large scale simulations of interaction of intense ultrashort laser pulses with molecular systems from fs for nuclear motion [5] to as for electron motion [6–8]. Ultrashort laser pulse advances have led to imaging pump-probe techniques such as laser Coulomb explosion imaging [5,9,10] for nuclear motion to laser-induced electron diffraction (LIED) [11–13] for coupled electron-nuclear motion. In LIED, the focus is on using near fs laser-induced electron scattering [14–18] to image molecular structure. Electrons have great potential for probing the time resolved transient structure of molecules, materials and even biological systems via ultrashort electron diffraction (UED) [19], and recent ultrashort laser pulses offer now the possibility of creating coherent electron wave packets inside molecules on the as time scale and subnanometer size [7,8,12] by the ultrashort intense phase-stabilized laser pulses [2–4]. UED [19] in molecules leads to interference phenomena predicted by Cohen and Fano [20] and Kaplan and Markin [21] for diatoms. In the present work, we present a numerical study of one-photon single ionization of H_2 with linear and circular polarization light using an exact numerical algorithm for solving the time-dependent Schrödinger equation (TDSE). We use a two-dimension (2D) model, restricting the two-electron motion in a plane in the Born-Oppenheimer approximation, i.e., with static nuclei. Such a 2D model has recently been use to study correlation effects on high-order harmonic generation (HHG) in H_2 using multiconfiguration methods [22]. In the present work, we solve numerically four-dimension (4D) partial differential equations for the two-electron motion necessitating large [terabyte size (10^{12} points)] grid for treating adequately the continuum electron motion and to extend calculations to high intensities to the nonlinear nonperturbative regime. We obtain the ionization angular distribution for the ground $X\ ^1\Sigma_g^+$ and excited $A\ ^3\Sigma_u^+$ states of the H_2 molecule at wavelengths 10 nm (ω=4.56 a.u.) and 5 nm (ω=9.1 a.u.) both at equilibrium, R_e=1.675 a.u. and for the extended (stretched) configuration at R=10 a.u.. At equilibrium, molecular orbitals, i.e., delocalized electron functions are adequate representations of the single electron whereas in the latter extended configuration, one expects the two electron-wave function to become localized Heitler-London atomic functions corresponding to valence-bond structures [23]. Recent experimental work in double photoionization in D_2 molecules [24] have shown methods to measure correlated electron ionization in coincidence with ion fragmentations. Recent time-resolved UED has been shown to be possible with transiently aligned molecules [25]. We present results of ionization for parallel and perpendicular alignment of H_2 with respect to the laser polarization axis. We also compare the photoionization of the ground $X\ ^1\Sigma_g^+$ state vs the excited $A\ ^3\Sigma_u^+$ state in order to investigate the role of exchange symmetry known to influence the ionization as a function of internuclear distance at high intensities in a previous nonperturbative one-dimension (1D) simulation [26]. Our simulations of 2D aligned H_2 complement previous three-dimension (3D) simulations of nonaligned ground state H_2^+, H_2, and Li_2^+ [27]. Alignment methods are currently well development [13,25] and will serve to elucidate interference effects in multicenter systems.

The 2D (plane) H_2 problem becomes a 4D partial differential equation with (ρ_1,θ_1) and (ρ_2,θ_2) polar coordinates for the two electrons [26]. The TDSE is appropriately written as (through this paper, atomic units, a.u., $e=\hbar=m_e=1$ are used unless otherwise noted),

$$i\frac{\partial}{\partial t}\psi(1,2)=\left[-\frac{1}{2}(\nabla_1^2+\nabla_2^2)+V_{ee}+V_{en}+V_L\right]\psi(1,2), \quad (1)$$

where $\nabla_{1,2}^2$ is the 2D Laplacian on the right hand side of Eq. (1), V_{ee} is the electron-electron repulsion and the electron-proton attraction Coulomb potentials is V_{en},

*andre.bandrauk@usherbrooke.ca

$$V_{ee} = \frac{1}{\sqrt{\rho_1^2 + \rho_2^2 - 2\rho_1\rho_2 \cos(\theta_1 - \theta_2) + \alpha}}, \tag{2}$$

$$V_{en} = -\sum_{j=1}^{2} \frac{1}{\sqrt{\rho_j^2 \pm R\rho_j + R^2/4 + \beta}}. \tag{3}$$

R is the internuclear distance between protons, α and β are regularization parameters to remove Coulomb singularities (this corresponds to averaging over the third dimension perpendicular to the plane of the molecule, i.e., the z direction). The laser-electron radiative coupling is described by the time dependent potential V_L, for a duration T laser pulse $E(t)$ for intensity $I_0 = \frac{1}{2}c\varepsilon_0 E_0^2$ with maximum amplitude E_0, pulse envelope $f(t)$ and frequency ω, for a parallel polarization,

$$V_L = -(\rho_1 \cos\theta_1 + \rho_2 \cos\theta_2) E_0 f(t) \cos\omega t, \tag{4}$$

and for perpendicular polarization,

$$V_L = -(\rho_1 \sin\theta_1 + \rho_2 \sin\theta_2) E_0 f(t) \sin\omega t, \tag{5}$$

and for circular polarized pulse

$$V_L = -E_0 f(t) \left[\sum_{j=1}^{2} (\rho_j \cos\theta_j \cos\omega t + \rho_j \sin\theta_j \sin\omega t) \right]. \tag{6}$$

We assume a temporal slowly varying envelope

$$f(t) = \sin^2(\pi t/T), \tag{7}$$

so that the total pulse area $\int E(t)dt = 0$ is thus constrained in accordance with Maxwell's equation [1]. We solve the 4D TDSE Eq. (1) by a third order split-operator method of third order accuracy in the time step δt and higher order in the spatial steps $\delta\rho$ and $\delta\theta$ [28]. Since the Laplacian's ∇_j^2 contain singularities at $\rho = 0$ in polar coordinates, we use the methodology as described in [26] to obtain the regularized 4D Laplacian propagator for the two electrons in H_2 insuring unitarity at each time step.

The regularization parameters are chosen to be $\alpha = 1.0$ and $\beta = 0.35$ allowing to reproduce the ground state and excited potential energy of the H_2 molecule accurately [29]. The ground $X\ ^1\Sigma_g^+$ state equilibrium distance is $R_e = 1.675$ a.u. with eigenenergy -1.3894 a.u.. The corresponding 4D values, $E(A\ ^3\Sigma_u^+) - E(X\ ^1\Sigma_g^+) = 0.35$ a.u. and dissociation energy $E(\infty) - E(X\ ^1\Sigma_g^+) = 0.19$ a.u., are in good agreement with the accurate values [30]. The time step is taken to be $\delta t = 0.01$ a.u. (1 a.u. = 24 as) and the spatial discretization is $\delta\rho = 0.25$ a.u. for a grid size $0 \le \rho \le 128$ a.u. and angle grid size $\delta\theta = 0.05$ a.u.. To prevent unphysical effects due to the reflection of the wave packet from the boundary, we multiply $\Psi(\mathbf{r}, t)$ by a "mask function" or absorber with the form

$$g(t) = \begin{cases} 1, & \rho < \rho_a, \\ \cos^{1/8}[\pi(\rho - \rho_a)/2\rho_{abs}], & \rho_a \le \rho \le \rho_{max}. \end{cases} \tag{8}$$

For all results reported here we set the absorber domain $\rho_{abs} = \rho_{max} - \rho_a$ at 24 a.u., exceeding well the field induced displacement $\alpha = E_0/\omega^2$ of the electron.

The two-electron time dependent function $\psi(\rho_1, \theta_1, \rho_2, \theta_2, t)$ allows for a study of the radial distribution $|\psi(\rho_1, \rho_2, t)|^2$ by integrating over angles θ_1 and θ_2, or the angular distribution $|\psi(\theta_1, \theta_2, t)|^2$ after integrating out the radial coordinates ρ_1 and ρ_2. In order to illustrate electron angular distribution spectra, a radial flux (electron current density) $\mathcal{J}(t)$ is employed. The total two-electron wave function $\psi(\rho_1, \theta_1, \rho_2, \theta_2, t)$ generates the radial flux $\mathcal{J}(t)$ at large distance ρ_0 before the wave packet is absorbed in polar coordinates. The electron angular distributions are reduced to one electron spectra by integrating out one electron, i.e.,

$$\mathcal{J}(\theta_2, t) = \frac{1}{2i} \left\{ \int\int d\rho_1 d\theta_1 \times \left[\psi^*(\rho_1, \theta_1, \rho_2, \theta_2, t) \frac{\partial \psi(\rho_1, \theta_1, \rho_2, \theta_2, t)}{\partial \rho_2} - \frac{\partial \psi^*(\rho_1, \theta_1, \rho_2, \theta_2, t)}{\partial \rho_2} \psi(\rho_1, \theta_1, \rho_2, \theta_2, t) \right]_{\rho_2 = \rho_0} \right\}, \tag{9}$$

with the corresponding angular differential yield

$$\mathcal{J}(\theta) = \int \mathcal{J}(\theta_2, t) dt. \tag{10}$$

We show first ionization angular distributions for H_2 at equilibrium distance, $R_e = 1.675$ a.u. for both ground $X\ ^1\Sigma_g^+$ and first excited $A\ ^3\Sigma_u^+$ electronic states at intensity $I_0 = 5 \times 10^{13}$ W/cm^2 and different excitation wavelengths $\lambda = 10$ nm in Fig. 1 and $\lambda = 5$ nm in Fig. 2. In Fig. 3, we show ionization angular distributions for the extended, $R = 10$ a.u., configuration at excitation wavelength $\lambda = 10$ nm. The choice of an equilibrium short distance, $R_e = 1.675$ a.u. and the extended configuration, $R = 10$ a.u. allows to compare changes in electron configuration. Thus, at equilibrium, the ground $X\ ^1\Sigma_g^+$ state is basically a 50% mixture of the symmetric covalent atomic Heitler-London configuration H···H,

$$\psi_1(1,2) = 1s_a(1)1s_b(2) + 1s_a(2)1s_b(1) \tag{11}$$

and the ionic configuration $H^+H^- + H^-H^+$

$$\psi_2(1,2) = 1s_a(1)1s_a(2) + 1s_b(1)1s_b(2) \tag{12}$$

obtained from the molecular orbital, MO configuration $1\sigma_g^2$ [23], whereas the triplet $A\ ^3\Sigma_u^+$ state described by the MO configuration $1\sigma_g 1\sigma_u$ is the antisymmetric covalent atomic configuration

$$\psi_3(1,2) = 1s_a(1)1s_b(2) - 1s_a(2)1s_b(1). \tag{13}$$

At large distance, both covalent configurations ψ_1 and ψ_3 dominate the two-electron wave function. Thus at large distance only a phase change in the entanglement via exchange of atomic electronic configurations $1s_a 1s_b$ differentiates the $X\ ^1\Sigma_g^+$ and $A\ ^3\Sigma_u^+$ states.

Both 2D angular distributions for the $X\ ^1\Sigma_g^+$ and $A\ ^3\Sigma_u^+$ states at equilibrium are in good agreement with the 3D distributions for the H_2 molecules using different numerical methods [31]. Figure 1 shows that for both the $X\ ^1\Sigma_g^+$ and

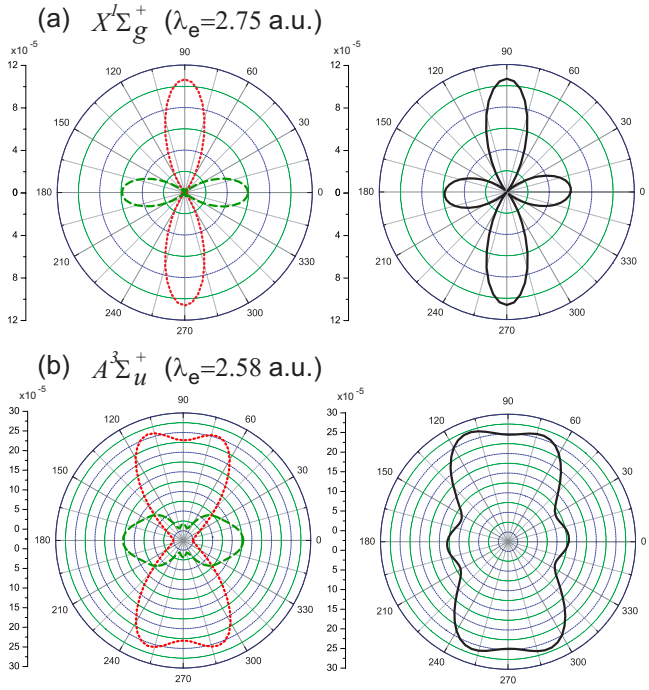

FIG. 1. (Color online) Ionization angular distributions in H_2 electronic states at photon wavelength $\lambda=10$ nm and intensity $I_0=5.0\times10^{13}$ W/cm^2 at equilibrium distance $R_e=1.675$ a.u.. (a) $X\ ^1\Sigma_g^+$, (b) $A\ ^3\Sigma_u^+$. Solid black line (—): circular polarization; dashed green line (- -): parallel linear polarization; and dotted red line (···): perpendicular linear polarization. The corresponding wavelengths λ_e of the ejected electron for the two electronic states are, respectively, 2.75 and 2.58 a.u. The units of angular distribution are arbitrary.

$A\ ^3\Sigma_u^+$ states at longer wavelengths such that the ionized-electron wavelength λ_e is greater than the internuclear distance R_e, the ionization angular distributions for circular polarization is basically the sum of orthogonal, i.e., parallel and perpendicular linear polarization angular distributions, thus confirming that in this case negligible diffraction is occurring. Figure 2 on the other hand where $\lambda_e \simeq R_e$, shows an asymmetry in the circular polarization angular distributions for both $X\ ^1\Sigma_g^+$ and $A\ ^3\Sigma_u^+$ states. This is due to more complex angular distribution for parallel and perpendicular linear polarization ionization rates which by themselves show no asymmetry. Thus, for this case where the ionized-electron wavelength is equal to the internuclear distance, circular polarization ionization angular distributions become asymmetric as seen in Figs. 2(a) and 2(b).

Figure 3 shows the ionization angular distributions for ionized electron wavelengths λ_e about 1/4 of the internuclear distance R. Both parallel and perpendicular linear polarization ionization angular distributions are very similar for both $X\ ^1\Sigma_g^+$ and $A\ ^3\Sigma_u^+$ states. The circular polarization rates however are no longer simple superpositions of parallel and perpendicular linear ionizations, thus, reflecting the different symmetry of the two electron Heitler-London covalent wave functions ψ_1 and ψ_3, Eqs. (11) and (13). This is to be compared to Figs. 1 and 2 at the equilibrium $R_e=1.675$ a.u. where no oscillations in the angular distributions occur. In Fig. 3(b) for the $A\ ^3\Sigma_u^+$ state, one observes eight peaks in the

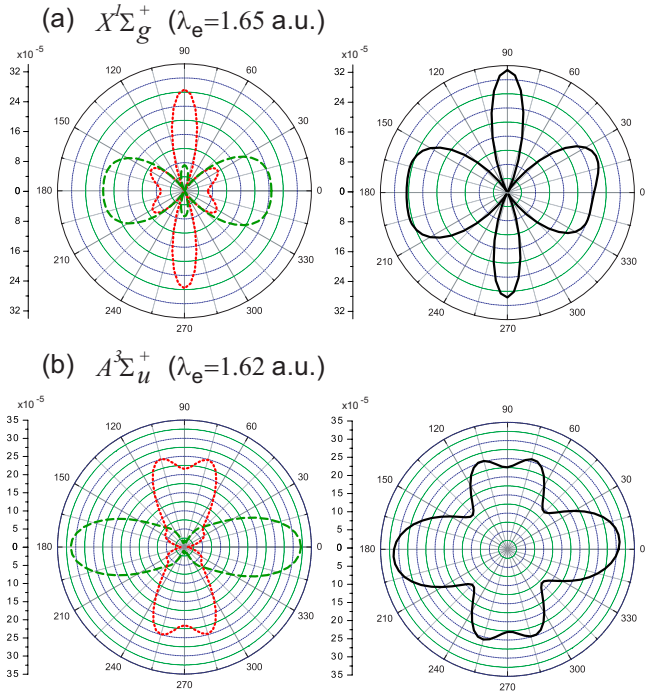

FIG. 2. (Color online) Same as Fig. 1, except for photon wavelength $\lambda=5$ nm. The wavelengths λ_e for the two electronic states are, respectively, 1.65 and 1.62 a.u.

circular polarization perpendicular distribution. This correlates with the fact that the internuclear distance $R=10$ a.u. is spanned by four wavelengths $\lambda_e=2.44$ a.u.. This interference is less pronounced in Fig. 3(a) for the $X\ ^1\Sigma_g^+$ state. The antisymmetry of the two-electron wave functions creates a

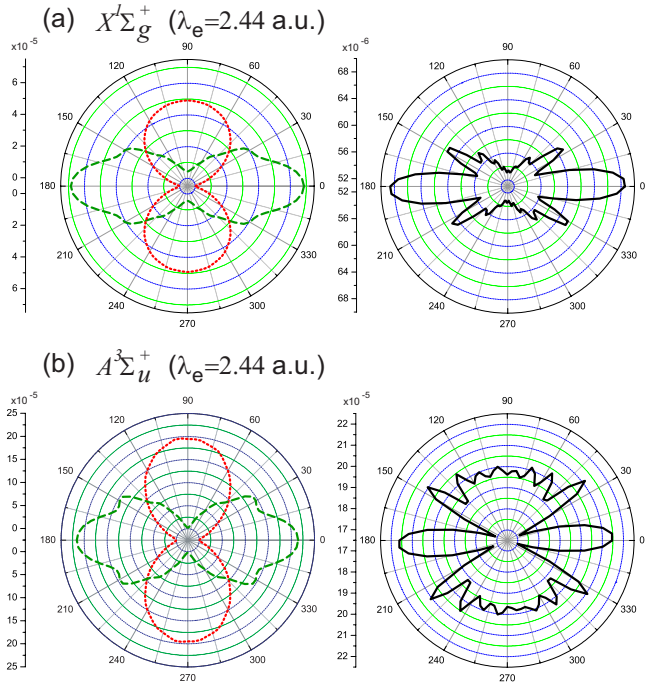

FIG. 3. (Color online) Same as Fig. 1, except for nuclear distance $R=10$ a.u.. Both wavelengths λ_e of the ejected electron for the two electronic states are 2.44 a.u.

different "entanglement" by exchange of the two electrons at large distance and this is reflected strongly in the circular polarization angular distributions shown in Fig. 3. In that figure, no interference appears in the perpendicular linear polarization (dotted red lines) angular distributions. As discussed in [27], no interference is expected in that case at emission angles $\sin\theta = n\lambda_e/R$ as observed in Figs. 1 and 2. In Fig. 3 since $R/\lambda_e \simeq 4$, one would now expect considerable interference based on the simple Young's interference model. However as seen from Eqs. (11) and (13) at $R=10$ a.u., one is now in the localized electron (Heitler-London) regime as compared to the delocalized molecular orbital regime at $R=R_e=1.675$ a.u., Figs. 1 and 2. It is in the delocalized molecular orbital regime that ionization interferences dominate [20,21]. The lack of interference in the perpendicular linear polarization results of Fig. 3 is therefore, indicative of the localized nature of the electrons through strong correlation. However for circularly polarized light, the entanglement of the electron pair via antisymmetry enhances the interference since electrons can be transferred from one center to the other by the action of the circular electric field.

In conclusion, we have shown that 2D numerical simulations of photoionization of H_2 by few cycle XUV laser pulses show enhanced interference effects via diffraction for circularly polarized pulses due to the concomitant interference between parallel and perpendicular ionization. The interference effects are further accentuated at large internuclear distances where entanglement of atomic configurations, corresponding to the Heitler-London wave functions, via exchange dominates. Imaging of orbital electron distributions has been previously achieved by electron momentum spectroscopy through binary $(e,2e)$ reactions [32]. Ultrashort few cycle XUV pulses allow for measuring ionization angular distributions at fixed molecular orientations and internuclear distances, and for distinguishing electron delocalization vs electron localization as a function of internuclear distance. We have shown that in the latter case, electron entanglement via exchange due to spin strongly influences ionization in circular polarization. Spin exchange entanglement is now considered an important tool for quantum computing via coupled quantum dots [33] and the present 2D H_2 simulations suggest a method of measuring electron entanglement as a function of internuclear distance.

[1] T. Brabec *et al.*, Rev. Mod. Phys. **72**, 545 (2000).
[2] P. Agostini *et al.*, Rep. Prog. Phys. **67**, 813 (2004).
[3] A. D. Bandrauk *et al.*, New J. Phys. **10**, 025004 (2008).
[4] F. Krausz *et al.*, Rev. Mod. Phys. **81**, 163 (2009).
[5] S. Chelkowski, P. B. Corkum, and A. D. Bandrauk, Phys. Rev. Lett. **82**, 3416 (1999).
[6] M. Spanner *et al.*, J. Phys. B **37**, L243 (2004).
[7] S. Chelkowski *et al.*, J. Phys. B **39**, S409 (2006).
[8] H. Niikura, D. M. Villeneuve, and P. B. Corkum, Phys. Rev. Lett. **94**, 083003 (2005).
[9] F. Légaré *et al.*, J. Phys. B **39**, S503 (2006).
[10] C. Cornaggia, in *Progress in Ultrafast Intense Laser Science*, edited by K. Yamanouchi *et al.* (Springer, New York, in press), Vol. V.
[11] T. Zuo *et al.*, Chem. Phys. Lett. **259**, 313 (1996).
[12] A. D. Bandrauk *et al.*, J. Phys. B **42**, 134001 (2009).
[13] M. Meckel *et al.*, Science **320**, 1478 (2008).
[14] P. B. Corkum, Phys. Rev. Lett. **71**, 1994 (1993).
[15] A. D. Bandrauk, S. Chelkowski, and S. Goudreau, J. Mod. Opt. **52**, 411 (2005).
[16] A. D. Bandrauk, S. Chelkowski, and I. Kawata, Phys. Rev. A **67**, 013407 (2003).
[17] M. Lein, J. P. Marangos, and P. L. Knight, Phys. Rev. A **66**, 051404(R) (2002).
[18] S. X. Hu and L. A. Collins, Phys. Rev. Lett. **94**, 073004 (2005).
[19] T. Morishita, A. T. Le, Z. Chen, and C. D. Lin, Phys. Rev. Lett. **100**, 013903 (2008).
[20] H. D. Cohen *et al.*, Phys. Rev. **150**, 30 (1966).
[21] I. G. Kaplan *et al.*, Sov. Phys. Dokl. **14**, 36 (1969).
[22] S. Sukiasyan, C. McDonald, C. Destefani, M. Y. Ivanov, and T. Brabec, Phys. Rev. Lett. **102**, 223002 (2009).
[23] C. F. Matta *et al.*, *The Quantum Theory of Atoms in Molecules* (Wiley, New York, 2009).
[24] R. Dörner *et al.*, Phys. Rev. Lett. **81**, 5776 (1998).
[25] P. Reckenthaeler *et al.*, Phys. Rev. Lett. **102**, 213001 (2009).
[26] A. D. Bandrauk *et al.*, in *High-Dimensional Partial Differential Equations in Science and Engineering*, edited by A. D. Bandrauk *et al.*, CRM Lecture Series Vol. 41 (American Math. Soc., Philadelphia, 2007), pp. 1–15.
[27] J. Fernández, F. L. Yip, T. N. Rescigno, C. W. McCurdy, and F. Martín, Phys. Rev. A **79**, 043409 (2009).
[28] A. D. Bandrauk *et al.*, J. Chem. Phys. **99**, 1185 (1993).
[29] A. D. Bandrauk and H. Z. Lu, Phys. Rev. A **72**, 023408 (2005); J. Phys. B **38**, 2529 (2005).
[30] W. Kołos, *et al.*, J. Chem. Phys. **43**, 2429 (1965); **45**, 509 (1966).
[31] S. X. Hu, L. A. Collins, and B. I. Schneider, Phys. Rev. A **80**, 023426 (2009).
[32] C. E. Brion *et al.*, Chem. Phys. **270**, 13 (2001).
[33] G. Burkard, D. Loss, and D. P. DiVincenzo, Phys. Rev. B **59**, 2070 (1999).